



27 the conducted experiments. The growth rate of the newly formed particles ranged from 3 – 11 nm
28 h^{-1} with particles reaching a diameter of 20-25 nm after a few hours. The nucleation rate was
29 estimated using an aerosol dynamics model and was found to be in the range of 500 to 25000
30 particles $\text{cm}^{-3} \text{h}^{-1}$ for the different experiments. These results support the hypothesis that ammonia
31 at levels of several ppb can accelerate or even cause new particle formation at least in the
32 environment of the Eastern Mediterranean.

33

34 **1. Introduction**

35 Atmospheric aerosol can be produced from many natural or anthropogenic sources and
36 plays a significant role in Earth's climate and in public health (Haywood and Boucher, 2000; Pope
37 et al., 2002). Aerosols can affect climate either by scattering and absorbing incoming solar
38 radiation (direct effect) or by acting as cloud condensation nuclei (CCN) thus affecting reflectivity
39 and lifetimes of clouds (indirect effect). New particle formations (NPF) through nucleation of low-
40 volatility vapors can be an important source of atmospheric aerosols and is responsible for close
41 to 50% of the global CCN (Merikanto et al., 2009). Newly formed particles either grow to larger
42 sizes through condensation or are scavenged by larger preexisting particles through coagulation.
43 Self-coagulation is another growth process for the newly formed particles. The competition
44 between these processes determines how many of those new particles will grow to become CCN
45 and how fast this will happen. NPF has been observed in many areas around the world including
46 all types of environments (urban, rural, forests, remote, marine, etc.) (Kulmala et al., 2007;
47 Kerminen et al., 2010; Wang et al., 2017; Yao et al., 2018; Zhu et al., 2019; Saha et al., 2019).

48 One of the challenges in studying the new particle formation process is the ability of the
49 available instrumentation to measure such small particles (Kulmala et al., 2012). Previous studies
50 have underlined the importance of sulfuric acid for NPF in most environments (Jaeger-Voirol and
51 Mirabel, 1989; Weber et al., 1996; Laaksonen et al., 2000; Sipila et al., 2010). Additional studies
52 have shown the importance of ammonia and amines as vapors that can accelerate the nucleation
53 rate of sulfuric acid with water by stabilizing the initial clusters of sulfuric acid. (Weber et al.,
54 1998; Kirkby et al., 2011; Jen et al., 2014; Glasoe et al., 2015). Low and extremely low volatility



55 organic vapors play a major role in the growth of the new particles and may be also participating
56 in the nucleation process itself (Yli-Juuti et al., 2011; Zhao et al., 2014; Ehn et al., 2014; Mohr et
57 al., 2019). In marine environments iodine compounds have been identified as vapors that can form
58 new particles (McFiggans et al., 2010; Sipilä et al., 2016; He et al., 2021) Wang et al. (2020) have
59 recently reported fast growth rates of newly formed particles at some atmospheric conditions due
60 to the condensation of ammonium nitrate. The preexisting aerosol (condensation sink), the
61 availability of gaseous precursors and the meteorological conditions all affect the intensity and
62 frequency of NPF events in the atmosphere.

63 Extensive monitoring of NPF events has taken place in many sites in Europe (Manninen et
64 al., 2010; Dinoi et al., 2021) and the eastern Mediterranean (Pikridas et al., 2012; Berland et al.,
65 2017; Kalkavouras et al., 2017; Kalivitis et al., 2019; Hussein et al., 2020; Brilke et al., 2020).
66 Siakavaras et al. (2016) reported frequent nucleation events in Thessaloniki, a major urban center
67 in northern Greece. On the other hand the nucleation frequency in southern Greece is relatively
68 low (compared to central and northern Europe) especially during the summer (Kalivitis et al.,
69 2008; 2019). Kopanakis et al. (2013) observed nucleation events only in 13 out of the 157 days of
70 measurements in the Akrotiri station, in Crete. Kalkavouras et al. (2020) reported a relatively low
71 20% nucleation frequency during the summer in Finokalia, Crete. Particle size distribution
72 measurements in five stations in Greece (Athens, Patras, Thessaloniki and Finokalia) during the
73 summer of 2012, showed low NPF frequency in Patras and Finokalia (Vratolis et al., 2019).
74 Pikridas et al. (2012) provided evidence that ammonia or amines may be the missing reactants that
75 are responsible for the lack of nucleation in this sunny relatively clean area with available sulfur
76 dioxide.

77 In this work we test the hypothesis that in an environment such as the Eastern
78 Mediterranean during the summer, under conditions favorable for nucleation (intense sunlight, low
79 to moderate particle concentrations, adequate sulfur levels) nucleation events are rare due to the
80 relatively low ammonia levels. The experiments took place during summer in Patras, Greece in
81 an environment with low regional nucleation frequency (Patoulas et al., 2018; Vratolis et al.,
82 2019) using a dual chamber system. Both chambers were filled with ambient air, ammonia was
83 added to one of them, and the evolution of the aerosol was followed in both chambers.

84
85



86 2. Methods

87 2.1 Dual chamber system

88 A dual chamber system was deployed as part of the 2019 summer PANACEA
89 (PANhellenic infrastructure for Atmospheric Composition and climatE change) campaign in
90 Patras, Greece. Measurements were conducted in the outskirts of Patras (population 200.000
91 people) between July 15 until August 15 2019, in the Institute of Chemical Engineering Sciences
92 (ICE-HT), approximately 8 km from the city center. The dual chamber system consisted of two
93 identical Teflon chambers (1.3 m³ each) located inside a structure that included the chambers and
94 five panels of UV lights used for illumination purposes ($J_{\text{NO}_2}=0.25 \text{ min}^{-1}$). Ammonia was added in
95 one of the chambers (perturbation chamber) while the other one was used as the reference. The top
96 of the structure can be removed and natural sunlight was used if the weather conditions allowed it.
97 Details about the design and testing of the dual chamber system can be found in Kaltsonoudis et
98 al. (2019).

99

100 2.2 Experimental procedure

101 Before the beginning of each experiment both chambers were flushed with ambient air
102 for approximately 2 hours. The main purpose of the flushing is the conditioning of the chambers
103 and the sampling lines to the environmental conditions and composition thus minimizing losses of
104 volatile or semivolatile compounds to the walls of the system. During this preparation period both
105 chambers were swept for 20 min using an ionizer fan (Dr Schneider PC, Model SL-001) to reduce
106 the charges on the chamber walls thus reducing the particle wall losses (Jorga et al., 2020). After
107 the chambers were ready, they were filled with ambient air using a metal-bellows pump (Senior
108 Aerospace, model MB-302). The concentrations of pollutants in both the gas and particulate phases
109 were then characterized for one hour. A 0.25 in copper tube was used for the particle phase
110 measurements and a 0.25 in PTFE tube was used for the gas measurements. The instruments were
111 located inside a room next to the chambers to avoid their exposure to high temperatures. The
112 distance from the chambers to the instruments was approximately 4 m. An automated valve was
113 used to alternate sampling between the two chambers. The valve was synchronized with the
114 sampling periods of the various instruments and sufficient time was allowed between each
115 sampling change to flush any remaining air from the previous measurement.



116 After the characterization phase, ammonia was injected through a heated line into the
117 perturbation chamber using a glass syringe. The concentration of the injected ammonia was
118 estimated using the volume of the chamber and the amount of liquid ammonia injected and it varied
119 from 20 to 200 ppb. After the ammonia injection, the top cover of the system was removed and
120 the chambers were exposed to natural sunlight. If the wind speed was high, the UV lights were
121 turned on, illuminating both chambers which remained covered.

122 At the end of the experiment, ammonium sulfate seeds were injected into both chambers
123 to measure the size dependent particle wall-loss rate constants using the method described in Wang
124 et al. (2018). After the end of the particle wall-losses period both chambers were flushed once
125 again with ambient air, to remove the ammonium sulfate and any remaining pollutants and to
126 prepare them for the next experiment.

127

128 **2.3 Instrumentation**

129 The chemical composition of the aerosol was monitored using a High Resolution Time-of-
130 Flight Aerosol Mass Spectrometer (HR-ToF-AMS) from Aerodyne Research Inc. Two Scanning
131 Mobility Particle Sizers (SMPS) were used to measure the number size distributions from 9-160
132 nm (classifier model 3080, CPC model 3775) and from 14-730 nm (classifier model 3080, CPC
133 model 3025A) respectively. The sample flow was dried before reaching the AMS and SMPS
134 systems using a nafion dryer. A suite of gas monitors were used to measure the concentrations of
135 NO_x (Teledyne 201E/501), SO₂ (Thermo Scientific Model 43i), and O₃ (Teledyne 400E).

136

137 **2.4 Aerosol dynamics model**

138 A zero-dimensional aerosol dynamic model was used for the simulation of nucleation,
139 condensation and coagulation inside the perturbation chamber (Capaldo et al., 1999). The
140 multicomponent aerosol size distribution is described using 270 size sections covering the
141 diameter range from 1 nm to 1 μm. The aerosol components include sulfate, ammonium, organics
142 and others with the latter assumed to be non-volatile and inert during the few hours of the
143 simulation period.

144 The condensation rate of H₂SO₄ to a particle of diameter D_p is described using the modified
145 form of the Fuchs-Sutugin equation (Hegg et al., 1991; Kreidenweis et al., 1991) given by:

146



147
$$J = 2\pi D D_p F(Kn) A (P - P_o) \quad (1)$$

148 where D is the diffusivity of the vapor air (set to $0.1 \text{ cm}^2 \text{ s}^{-1}$ in this application), Kn is the Knudsen
149 number (that is the ratio of the air mean free path to the particle radius), $F(Kn)$ is a coefficient
150 correcting for free molecular effects given by:

151
$$F(Kn) = \frac{1+Kn}{1+1.71Kn+1.33Kn^2} \quad (2)$$

152 and A is a coefficient correcting for the interfacial mass transport limitations described by the
153 accommodation α_e ,

154
$$A = \left[1 + 1.33Kn F(Kn) \left(\frac{1}{\alpha_e} - 1 \right) \right]^{-1} \quad (3)$$

155 Finally, P is the bulk H_2SO_4 vapor partial pressure and P_o is its partial pressure at the particle
156 surface. An accommodation coefficient of 0.02 for the condensation of H_2SO_4 on the aerosol
157 particles is assumed (Van Dingenen and Raes, 1991). The vapor pressure of H_2SO_4 at the aerosol
158 surface can be estimated from the data of Bolsaitis and Elliott (1990). Values less than 10^{-3} ppt
159 were found for the conditions of our experiments and therefore the surface vapor pressure of H_2SO_4
160 in our mass transfer calculations was assumed to be zero.

161 Brownian coagulation between all particles is simulated solving the discrete coagulation
162 equation (Seinfeld and Pandis, 2016) :

163
$$\frac{dN_k(t)}{dt} = \frac{1}{2} \sum_{j=1}^{k-1} K_{j,k-j} N_j N_{k-j} - N_k \sum_{j=1}^{\infty} K_{k,j} N_j \quad k \geq 2 \quad (4)$$

164 The generalized coagulation coefficient $K_{1,2}$ for the collision of two particles is calculated as:

165
$$K_{1,2} = 2\pi(D_1 + D_2)(D_{p1} + D_{p2})\beta \quad (5)$$

166 where D_1, D_2 are the individual Brownian diffusion coefficient for the particles, D_{p1}, D_{p2} are the
167 particle diameters and β is the Fuchs correction factor (Fuchs, 1964). Because of the high
168 resolution of the size distribution, coagulation can be simulated accurately by calculating directly
169 the coagulation rates between each of the size sections and moving the particles to the
170 corresponding size bin.

171

172



173 2.5 Data analysis

174 The condensation sink (CS) is a metric of the ability of the pre-existing aerosol population
175 to remove vapors from the system by condensation. The CS values were calculated using the
176 aerosol distribution between 14-700 nm, as measured by the SMPS and the properties of sulfuric
177 acid as the condensing vapor. The CS is given by:

$$178 \quad CS = 2\pi D \sum_i \beta_{mi} D_{pi} N_i \quad (6)$$

179 where D is the diffusion coefficient of sulphuric acid, β_m is the transition-regime correction factor,
180 D_p the diameter of the particle and N the respective number concentration in each size bin of the
181 SMPS.

182 Using the initial SO_2 concentration in the perturbed chamber and the condensation sink we
183 can estimate the sulfuric acid concentration according to:

$$184 \quad [\text{H}_2\text{SO}_4] = k_{OH} \frac{[\text{SO}_2][\text{OH}]}{CS} \quad (7)$$

185 where k_{OH} is the reaction constant of SO_2 and OH which is equal to $8.5 \times 10^{-13} \text{ cm}^3 \text{ molecule}^{-1} \text{ s}^{-1}$
186 at 298 K (Demore et al., 1997), $[\text{SO}_2]$ and $[\text{OH}]$ are the concentrations of sulphur dioxide and
187 hydroxyl radicals respectively, and CS is the condensational sink as calculated from Equation 7.
188 For the hydroxyl radical concentration, we assumed an average value of $5 \times 10^6 \text{ molecules cm}^{-3}$.
189 Equation (7) is based on the assumptions that the only sulfuric acid source is the oxidation of SO_2
190 from OH radicals, its major sink is its condensation onto the aerosol surface, and the system is at
191 pseudo-steady state.

192

193 3. Results and discussion

194 3.1 Initial conditions

195 Thirteen perturbation experiments were conducted during the study (Table 1). Two of them
196 took place during the night using UV lights and the rest during midday. Natural sunlight was used
197 in two experiments while UV lights were used during the rest.

198 The main components of non-refractory PM_{10} in the beginning of our experiments were
199 organics ($46.6 \pm 6.5\%$) followed by sulfate ($37.1 \pm 4.5\%$), ammonium ($14.3 \pm 1.8\%$), nitrate
200 ($1.5 \pm 0.5\%$) and chloride ($0.5 \pm 0.4\%$). The average oxygen to carbon ratio (O:C) (Canagaratna et
201 al., 2015) in the chambers after filling them with ambient air was 0.68 ± 0.1 , indicating an already



202 oxidized OA. In order to check if any contamination was occurring during the flushing and filling
203 processes we calculated the theta angle (Kostenidou et al., 2009) between the organic mass spectra
204 of the ambient air and the OA in the two chambers. The theta angles were less than 6° in all
205 experiments, indicating negligible contamination during the filling process.

206 The initial concentration of the SO_2 , NH_3 , O_3 and NO_x inside the chambers after the filling
207 process were approximately within 10% of their ambient values. The initial concentrations of these
208 gases in the two chambers differed by less than 3%. More than 70% of the ambient PM_{10} was
209 transferred in the chambers in most experiments. The initial PM_{10} levels were quite low ranging
210 from 0.6 to $4.2 \mu\text{g m}^{-3}$. The atmosphere of Patras was quite clear during these experiments. The
211 initial conditions in all experiments are summarized in Table 1.

212

213 3.2 New particle formation and growth

214 The conducted experiments were classified in three different classes based on the
215 observations of new particle formation in the two chamber. In class A experiments, nucleation and
216 particle growth occurred in only the perturbed chamber, in class B nucleation and particle growth
217 happened in both chambers and in class C when there was no detection of new particle formation
218 in either chamber.

219

220 3.2.1 Nucleation and growth only in the perturbed chamber

221 Nucleation and growth of the new particles to sizes above 9 nm only in the observations of
222 new particle formation. Figure 1 depicts the particle number concentration N_9 ($D_p > 9$ nm) after
223 corrections for losses to the chamber walls and the sampling lines, inside the two chambers for a
224 typical Class A experiment. During Exp. A1 the initial concentration of SO_2 was 0.7 ppb and of
225 O_3 equal to 58 ppb. After the injection of ammonia (approximately 150 ppb) the UV lights were
226 turned on ($t=0$ h) illuminating both chambers. The N_9 particle number concentration start
227 increasing in the perturbed chamber approximately 1.5 h after the lights were turned on, reaching
228 close to 4000 cm^{-3} , almost double its initial concentration value. The N_9 concentration in the
229 control chamber remained within 5% of the initial levels. Figure 2 shows the measured number
230 distributions in the two chambers after correction for particle losses. The formation and growth of
231 the new particles in the perturbed chamber is evident. With a CS of 0.0026 s^{-1} the H_2SO_4
232 concentration was calculated to be of the order of $3 \times 10^7 \text{ molecules cm}^{-3}$. Assuming that nucleation



233 started at $t=0$ the measured initial growth rate in the perturbed chamber was on average 4 nm h^{-1} .
234 This rate is based on the time of growth of the nucleation mode to 15 nm . For this experiment 3.8
235 h were required for the growth of the new particles to 15 nm so the estimated growth rate is
236 approximately 4 nm h^{-1} . The newly formed particles at the end of the experiment (after 5 h from
237 the illumination) grew to approximately 20 nm . The experiment was stopped at that point because
238 a significant fraction of the air in the two chambers had been sampled.

239 The estimated initial growth rates for the daytime experiments A1, A2, A4, A5, and A6
240 varied from 3.5 to 8 nm h^{-1} and were correlated with the estimated H_2SO_4 levels ($R^2=0.76$) (Table
241 2). Experiments A1, A5 and A6 had similar CS and H_2SO_4 levels and resulted in similar initial
242 growth rates (Table 2). The slope of the growth rate versus sulphuric acid linear regression for the
243 daytime experiments was $1.4 (\text{nm h}^{-1} \text{ molecule}^{-1} \text{ s})$ and the intercept was low and equal to 0.05 nm
244 h^{-1} .

245 Experiment A3 was conducted during the night (the chambers were filled with ambient air
246 at $21:00$ so it has relatively different behaviour than the rest. If this experiment is included in the
247 growth rate versus H_2SO_4 correlation, the R^2 drops to 0.27 . This probably suggests that the
248 estimated OH levels are not accurate in this case and therefore the H_2SO_4 is probably also a lot
249 more uncertain than in the other experiments. Also, the growth process may be different with
250 organic vapors playing a more significant role.

251

252 **3.2.2 Nucleation and growth in both chambers**

253 In 4 (B1 to B4) out of the 13 perturbation experiments, new particle formation and growth
254 was observed in both chambers (Table 2). This suggests that the ambient air had already the
255 potential to form new particles without the addition of ammonia.

256 Figure 1b shows the N_9 concentration in the two chambers during Exp. B1. The initial
257 levels of SO_2 in both chambers were 0.8 ppb and approximately 150 ppb of ammonia were added
258 to the perturbation chamber. Half hour after the exposure of the chambers to UV light the N_9 in
259 both chambers started increasing with higher concentrations in the perturbed chamber. The number
260 concentration of the particles in the perturbed chamber reached close to 6000 cm^{-3} almost three
261 times the initial levels. The concentration in the baseline chamber increased by approximately 50%
262 to 3000 cm^{-3} . The newly formed particles in the perturbed chamber at the end of the experiment
263 reached a mode diameter of 26 nm (Fig. 3) with an initial GR of 5.5 nm h^{-1} . The growth rate of the



264 particles in the reference chamber was only 10% lower than in the perturbed one (Fig. 4)
265 suggesting that the addition of ammonia probably influenced significantly the nucleation rate but
266 had a small effect on the growth rate.

267 We tested the hypothesis that the appearance of the new particles in the reference chamber
268 was due to a sampling error, caused by some cross contamination of the two samples as the same
269 sampling line was used. We compared the shape of aerosol size distributions in the two chambers.
270 The nucleation mode distribution in the reference chamber was wider (Figure S1), a strong
271 indication that these were different particle populations sampled by our system.

272 The condensation sink in the class B experiments was on average 0.0024 s^{-1} quite similar
273 to the 0.0023 s^{-1} in the A experiments so the pre-existing particle mass was quite similar in the two
274 classes of experiments. Also the average SO_2 was practically the same (0.83 ppb for the B
275 experiments and 0.82 ppb for the A experiments). Adding the similarity of the UV intensity, it is
276 clear that the major factors (sunlight, condensational sink, SO_2 availability) usually determining
277 nucleation rates were not the reason for the weak nucleation and growth in the reference chamber
278 in these experiments. Unfortunately, we did not have available accurate ammonia measurements,
279 because the presence of sufficient ammonia levels is one of the possible explanations for this
280 behaviour.

281 The observed growth rates in these B-class experiments varied from 3.5 to 11.3 nm h^{-1} and
282 were a little higher on average than those in the A group of experiments. Adding these four
283 experiments to the linear regression of the growth rate versus sulphuric acid reduced the R^2 to 0.43,
284 but the slope remained the same, while the intercept increased to 0.7 nm h^{-1} . These provide some
285 weak evidence of the involvement of more compounds, probably organics, in the growth of these
286 newly formed particles in this second group of experiments.

287

288 **3.2.2 Nucleation and growth not observed**

289 In three of the experiments C1-C3, we did not observe growth of new particles to the size
290 of 9 nm. It is still possible that there was nucleation, but the growth may have been too slow (less
291 than 2 nm h^{-1}). Figure 1c depicts the N_9 number concentration during Exp. C1. The initial
292 concentration of SO_2 was 1.3 ppb in this experiment. The number concentration after correction
293 for particle losses remained constant at close to 2200 cm^{-3} and the corresponding number
294 distributions changed little during the experiment (Fig. 4). Exp. C1 had the lowest initial levels of



295 ozone of all the experiments (Table 1), around 12 ppb, a factor of four lower than the average
296 concentration. The low O₃ levels were probably due to the highest NO_x levels (27 ppb) in this air
297 mass.

298 Exp. C2 was conducted in the early evening (the chamber was filled with ambient air
299 around 19:00 LT) and the lowest detectable particle size for this experiment was 14 nm because
300 of technical difficulties. Finally, Exp. C3 had relatively low levels of sulfuric acid (2.5×10^7
301 molecules cm⁻³) compared to the rest of the experiments, a low estimated level of injected ammonia
302 (20 ppb) and natural sunlight.

303

304 **3.3 Particle composition**

305 The mass concentration of the major components of PM₁ (sulfate, organics, nitrate,
306 ammonium) in the two chambers, after correcting for chamber particle wall losses, remained
307 practically constant during all experiments. The corrected for wall losses mass concentration inside
308 both chambers during Exp. B1 are shown in Figure 5. Taking into account the uncertainty of the
309 wall loss correction, the maximum production of the corresponding secondary PM components
310 during the few hours of the experiments should have been a few percent or less. This will be an
311 important constraint for the analysis of these experimental results with the aerosol dynamics model
312 in the next section.

313

314 **3.4 Estimation of nucleation rate using an aerosol dynamics model**

315 We used our aerosol dynamics model to simulate the growth and coagulation of the
316 particles in the perturbed chamber assuming a nucleation rate. Our goal is to use the observations
317 to constrain the nucleation rate that could not be measured directly. The model uses as inputs the
318 temperature and relative humidity during the experiments and is initialized with the measured
319 particle number distribution at time zero. There are three adjustable parameters in the model: the
320 duration of nucleation, the nucleation rate and the condensation rate. Nucleation is assumed to start
321 at time zero and a constant nucleation rate is assumed for the duration of the event. The condensing
322 components are assumed to have practically zero vapor pressure. The three parameters were
323 chosen so that the model predictions were in good agreement with the observations of particle
324 number concentration and size distribution and also the mass concentration.



325 Figure 6 shows the measured and the predicted particle number, surface and volume
326 concentrations in the perturbed chamber for Exp. A1. A nucleation event with rate equal to
327 $J_1=9500 \text{ cm}^{-3} \text{ h}^{-1}$ and duration of 3 h together with a condensation rate of 3.2 ppt h^{-1} was needed
328 to reproduce the observations. For much lower condensation rates the particles did not grow to
329 detectable sizes and for higher condensation rates the predicted PM mass increase was not
330 consistent with the small observed mass concentration change. We performed sensitivity analysis
331 around these central values and values of $J_1=9500\pm 600 \text{ cm}^{-3} \text{ h}^{-1}$ remained consistent with the
332 observations. The average errors during the simulation were 6% for the number concentration,
333 16% for the surface concentration and 17% for the mass concentration.

334 The predicted and observed evolution of the aerosol number distributions are shown in
335 Figure S2. The differences for the smaller particle sizes are partially due to the losses of these
336 particles in the sampling and measurement systems.

337 Table 3 summarizes the estimated nucleation rates together with the corresponding
338 durations of the nucleation events and the required condensation rates for all experiments in groups
339 A and B in which nucleation and growth were observed. The estimate J_1 rates varied from 500 to
340 $25000 \text{ cm}^{-3} \text{ h}^{-1}$.

341 These results can be roughly compared to the CLOUD measurements for sulfuric acid-
342 ammonia nucleation (Kirkby et al., 2011) in the 2×10^7 - 10^8 molecules cm^{-3} H_2SO_4 concentration
343 range that was estimated for our experiments. The CLOUD measurements for the highest ammonia
344 levels used suggested a $J_{1.7}$ rate of approximately $500 \text{ cm}^{-3} \text{ h}^{-1}$ for H_2SO_4 concentration equal to
345 5×10^7 molecules cm^{-3} . For experiment A4 we estimated the same H_2SO_4 concentration and a
346 nucleation rate of $400\pm 200 \text{ cm}^{-3} \text{ h}^{-1}$ (Fig. S3). While this agreement is probably fortuitous, overall
347 our estimated nucleation rates are in general consistent (considering their uncertainties) with the
348 CLOUD measurements for the ammonia-sulfuric acid system assuming that the rate does not
349 increase further as ammonia increases above 1 ppb.

350

351 4. Conclusions

352 A dual chamber system was used to investigate the hypothesis that ammonia is often the
353 limiting reactant for new particle formation in the Eastern Mediterranean. Ambient air
354 characterized by relatively aged air masses in southern Greece was used as the starting point of
355 our experiments. Ammonia was added in one chamber while the second was used as a reference.



356 In 6 out of the 13 experiments (46%) the addition of ammonia led to the formation and
357 then growth to detectable size (approximately 10 nm) of new particles, while no formation of
358 particles was observed in the reference chamber. In another 4 experiments (31%) the addition of
359 ammonia enhanced significantly the formation of new particles, but new particles were formed
360 also in the reference chamber. Finally, in the remaining 3 experiments (23%) we could not observe
361 new particle formation. New particles may have been formed and may have not grown to
362 detectable sizes in these experiments. The formed particles grew to sizes around 20-25 nm after 5
363 hours, with an estimated initial growth rate ranging from 3 to 11 nm h⁻¹. These results suggest that
364 the presence of ammonia, at least at the high levels used in our study, allowed almost half of the
365 time the formation and growth of particles that would not be formed otherwise. In one quarter of
366 the cases ammonia increased significantly the nucleation rate compared to the ambient conditions.
367 Finally, in the last quarter of the cases the high ammonia levels did not cause nucleation and growth
368 to detectable sizes.

369 We should note that we did not observe ammonium nitrate formation in any of our
370 experiments despite the high ammonia levels. This is probably due to the combination of relatively
371 low nitric acid levels and high temperatures during our study. This means that ammonium nitrate
372 was not involved in the formation and growth processes in this environment.

373 An aerosol dynamics model was used to estimate the J_1 nucleation rate constrained by the
374 measured aerosol number distribution and mass concentrations. The nucleation rate in the
375 perturbed chamber ranged from 500 cm⁻³ h⁻¹ up to 25000 cm⁻³ h⁻¹. Coupled with the estimated
376 sulfuric acid concentrations these rates are in general consistent (within one order of magnitude)
377 with the CLOUD measurements for the nucleation rates in the sulfuric acid-ammonia-water
378 system.

379 Experiments in which new particles formation was observed in both chambers show one
380 of the advantages of using a dual chamber system in such experiments. The use of the reference
381 chamber can help verify if the conducted perturbation was responsible for the observed change.
382 Future experiments with this system should include measurements of the sub-10 nm part of the
383 aerosol size distribution and accurate measurements of the NH₃ concentration.

384

385 **Data and code availability.** The laboratory results and the aerosol dynamics code are available
386 from the authors (spyros@chemeng.upatras.gr).



387 **Supplement.**

388

389 **Author contributions.** SDJ performed the experiments, analyzed the results and wrote the paper.
390 KF helped in the performance of the experiments. DP wrote the aerosol dynamics code. SNP was
391 responsible for the design of the study and the synthesis of the results and contributed to the writing
392 of the paper.

393

394 **Competing interests.** The authors declare that they have no conflict of interest.

395

396 **Financial support:** This work was supported by the project FORCeS funded from the European
397 Union's Horizon 2020 research and innovation programme under grant agreement No 821205. We
398 also acknowledge support by the Panhellenic infrastructure for atmospheric composition and
399 climate change (PANACEA) project (grant no. MIS 5021516), which is implemented under the
400 framework of "Reinforcement of the Research and Innovation Infrastructure" project funded by
401 the European Operational Programme of "Competitiveness, Entrepreneurship and Innovation"
402 (grant no. NSRF 2014–2020) and cofinanced by Greece and the European Union (as part of the
403 European Regional Development Fund).

404

405 **5. References**

406 Berland, K., Rose, C., Pey, J., Culot, A., Freney, E., Kalivitis, N., Kouvarakis, G., Cerro, J. C.,
407 Mallet, M., Sartelet, K., Beckmann, M., Bourriane, T., Roberts, G., Marchand, N.,
408 Mihalopoulos, N., and Sellegri, K.: Spatial extent of new particle formation events over
409 the Mediterranean Basin from multiple ground-based and airborne measurements, *Atmos.*
410 *Chem. Phys.*, 17, 9567–9583, <https://doi.org/10.5194/acp-17-9567-2017>, 2017.

411 Bolsaitis, P. and Elliott, J. F.: Thermodynamic activities and equilibrium partial pressures for
412 aqueous sulfuric acid solutions, *J. Chem. Eng. Data*, 35, 69–85, <https://doi.org/10.1021/je00059a022>, 1990.

414 Brilke, S., Fölker, N., Müller, T., Kandler, K., Gong, X., Peischl, J., Weinzierl, B., and Winkler,
415 P. M.: New particle formation and sub-10 nm size distribution measurements during the
416 A-LIFE field experiment in Paphos, Cyprus, *Atmos. Chem. Phys.*, 20, 5645–5656,
417 <https://doi.org/10.5194/acp-20-5645-2020>, 2020.



- 418 Canagaratna, M. R., Jimenez, J. L., Kroll, J. H., Chen, Q., Kessler, S. H., Massoli, P., Hildebrandt
419 Ruiz, L., Fortner, E., Williams, L. R., Wilson, K. R., Surratt, J. D., Donahue, N. M., Jayne,
420 J. T., and Worsnop, D. R.: Elemental ratio measurements of organic compounds using
421 aerosol mass spectrometry: characterization, improved calibration, and implications,
422 *Atmos. Chem. Phys.*, 15, 253–272, <https://doi.org/10.5194/acp-15-253-2015>, 2015.
- 423 Capaldo, K. P., Kasibhatla, P., and Pandis, S. N.: Is aerosol production within the remote marine
424 boundary layer sufficient to maintain observed concentrations?, *J. Geophys. Res.*, 104,
425 3483–3500, <https://doi.org/10.1029/1998JD100080>, 1999.
- 426 Demore, W. B., Sander, S. P., Golden, D. M., Hampson, R. F., Kurylo, M. J., Howard, C. J.,
427 Ravishankara, A. R., Kolb, C. E., and Molina, M. J.: Chemical Kinetics and Photochemical
428 Data for Use in Stratospheric Modeling Evaluation Number 12 NASA Panel for Data
429 Evaluation, 1997.
- 430 Van Dingenen, R. and Raes, F.: Determination of the condensation accommodation coefficient of
431 sulfuric acid on water-sulfuric acid aerosol, *Aerosol Sci. Technol.*, 15, 93–106,
432 <https://doi.org/10.1080/02786829108959516>, 1991.
- 433 Dinoi, A., Weinhold, K., Wiedensohler, A., and Contini, D.: Study of new particle formation
434 events in southern Italy, *Atmos. Environ.*, 244, 117920, [https://doi.org/10.1016/](https://doi.org/10.1016/j.atmosenv.2020.117920)
435 [j.atmosenv.2020.117920](https://doi.org/10.1016/j.atmosenv.2020.117920), 2021.
- 436 Ehn, M., Thornton, J. A., Kleist, E., Sipilä, M., Junninen, H., Pullinen, I., Springer, M., Rubach,
437 F., Tillmann, R., Lee, B., Lopez-Hilfiker, F., Andres, S., Acir, I. H., Rissanen, M., Jokinen,
438 T., Schobesberger, S., Kangasluoma, J., Kontkanen, J., Nieminen, T., Kurtén, T., Nielsen,
439 L. B., Jørgensen, S., Kjaergaard, H. G., Canagaratna, M., Maso, M. D., Berndt, T., Petäjä,
440 T., Wahner, A., Kerminen, V. M., Kulmala, M., Worsnop, D. R., Wildt, J., and Mentel, T.
441 F.: A large source of low-volatility secondary organic aerosol, *Nature*, 506, 476–479,
442 <https://doi.org/10.1038/nature13032>, 2014.
- 443 Glasoe, W. A., Volz, K., Panta, B., Freshour, N., Bachman, R., Hanson, D. R., McMurry, P. H.,
444 and Jen, C.: Sulfuric acid nucleation: An experimental study of the effect of seven bases,
445 *J. Geophys. Res. Atmos.*, 120, 1933–1950, <https://doi.org/10.1002/2014JD022730>, 2015.
- 446 Haywood, J. and Boucher, O.: Estimates of the direct and indirect radiative forcing due to
447 tropospheric aerosols: A review, *Rev. Geophys.*, 38, 513–543, [https://doi.org/10.1029/](https://doi.org/10.1029/1999RG000078)
448 [1999RG000078](https://doi.org/10.1029/1999RG000078), 2000.



- 449 He, X.-C., Tham, Y. J., Dada, L., Wang, M., Finkenzeller, H., Stolzenburg, D., Iyer, S., Simon,
450 M., Kürten, A., Shen, J., Rörup, B., Rissanen, M., Schobesberger, S., Baalbaki, R., Wang,
451 D. S., Koenig, T. K., Jokinen, T., Sarnela, N., Beck, L. J., Almeida, J., Amanatidis, S.,
452 Amorim, A., Ataei, F., Baccarini, A., Bertozzi, B., Bianchi, F., Brilke, S., Caudillo, L.,
453 Chen, D., Chiu, R., Chu, B., Dias, A., Ding, A., Dommen, J., Duplissy, J., El Haddad, I.,
454 Gonzalez Carracedo, L., Granzin, M., Hansel, A., Heinritzi, M., Hofbauer, V., Junninen,
455 H., Kangasluoma, J., Kemppainen, D., Kim, C., Kong, W., Krechmer, J. E., Kvashin, A.,
456 Laitinen, T., Lamkaddam, H., Lee, C. P., Lehtipalo, K., Leiminger, M., Li, Z., Makhmutov,
457 V., Manninen, H. E., Marie, G., Marten, R., Mathot, S., Mauldin, R. L., Mentler, B.,
458 Möhler, O., Müller, T., Nie, W., Onnela, A., Petäjä, T., Pfeifer, J., Philippov, M.,
459 Ranjithkumar, A., Saiz-Lopez, A., Salma, I., Scholz, W., Schuchmann, S., Schulze, B.,
460 Steiner, G., Stozhkov, Y., Tauber, C., Tomé, A., Thakur, R. C., Väisänen, O., Vazquez-
461 Pufleau, M., Wagner, A. C., Wang, Y., Weber, S. K., Winkler, P. M., Wu, Y., Xiao, M.,
462 Yan, C., Ye, Q., Ylisirniö, A., Zauner-Wieczorek, M., Zha, Q., Zhou, P., Flagan, R. C.,
463 Curtius, J., Baltensperger, U., Kulmala, M., Kerminen, V.-M., Kurtén, T., et al.: Role of
464 iodine oxoacids in atmospheric aerosol nucleation, *Science*, 371, 589–595, 2021.
- 465 Hegg, D. A., Radke, L. F., and Hobbs, P. V.: Measurements of Aitken nuclei and cloud
466 condensation nuclei in the marine atmosphere and their relation to the DMS-Cloud-climate
467 hypothesis, *J. Geophys. Res.*, 96, 18727, <https://doi.org/10.1029/91JD01870>, 1991.
- 468 Hussein, T., Atashi, N., Sogacheva, L., Hakala, S., Dada, L., Petäjä, T., and Kulmala, M.:
469 Characterization of urban new particle formation in Amman-Jordan, *Atmosphere (Basel)*,
470 11, 79, <https://doi.org/10.3390/atmos11010079>, 2020.
- 471 Jaecker-Voirol, A. and Mirabel, P.: Heteromolecular nucleation in the sulfuric acid-water system,
472 *Atmos. Environ.*, 23, 2053–2057, [https://doi.org/10.1016/0004-6981\(89\)90530-1](https://doi.org/10.1016/0004-6981(89)90530-1), 1989.
- 473 Jen, C. N., McMurry, P. H., and Hanson, D. R.: Stabilization of sulfuric acid dimers by ammonia,
474 methylamine, dimethylamine, and trimethylamine, *J. Geophys. Res.*, 119, 7502–7514,
475 <https://doi.org/10.1002/2014JD021592>, 2014.
- 476 Jorga, S. D., Kaltsonoudis, C., Liangou, A., and Pandis, S. N.: Measurement of formation rates of
477 secondary aerosol in the ambient urban atmosphere using a dual smog chamber system,
478 *Environ. Sci. Technol.*, 54, 1336–1343, <https://doi.org/10.1021/acs.est.9b03479>, 2020.
- 479 Kalivitis, N., Birmili, W., Stock, M., Wehner, B., Massling, A., Wiedensohler, A., Gerasopoulos,



- 480 E., and Mihalopoulos, N.: Particle size distributions in the Eastern Mediterranean
481 troposphere, *Atmos. Chem. Phys.*, 8, 6729–6738, [https://doi.org/10.5194/acp-8-6729-](https://doi.org/10.5194/acp-8-6729-2008)
482 2008, 2008.
- 483 Kalivitis, N., Kerminen, V. M., Kouvarakis, G., Stavroulas, I., Tzitzikalaki, E., Kalkavouras, P.,
484 Daskalakis, N., Myriokefalitakis, S., Bougiatioti, A., Manninen, H. E., Roldin, P., Petäjä,
485 T., Boy, M., Kulmala, M., Kanakidou, M., and Mihalopoulos, N.: Formation and growth
486 of atmospheric nanoparticles in the eastern Mediterranean: Results from long-term
487 measurements and process simulations, *Atmos. Chem. Phys.*, 19, 2671–2686,
488 <https://doi.org/10.5194/acp-19-2671-2019>, 2019.
- 489 Kalkavouras, P., Bossioli, E., Bezantakos, S., Bougiatioti, A., Kalivitis, N., Stavroulas, I.,
490 Kouvarakis, G., Protonotariou, A. P., Dandou, A., Biskos, G., Mihalopoulos, N., Nenes,
491 A., and Tombrou, M.: New particle formation in the southern Aegean Sea during the
492 Etesians: Importance for CCN production and cloud droplet number, *Atmos. Chem. Phys.*,
493 17, 175–192, <https://doi.org/10.5194/acp-17-175-2017>, 2017.
- 494 Kalkavouras, P., Bougiatioti, A., Grivas, G., Stavroulas, I., Kalivitis, N., Liakakou, E.,
495 Gerasopoulos, E., Pilinis, C., and Mihalopoulos, N.: On the regional aspects of new particle
496 formation in the Eastern Mediterranean: A comparative study between a background and
497 an urban site based on long term observations, *Atmos. Res.*, 239, 104911,
498 <https://doi.org/10.1016/j.atmosres.2020.104911>, 2020.
- 499 Kaltsonoudis, C., Jorga, S. D., Louvaris, E., Florou, K., and Pandis, S. N.: A portable dual-smog-
500 chamber system for atmospheric aerosol field studies, *Atmos. Meas. Tech.*, 12, 2733–2743,
501 <https://doi.org/10.5194/amt-12-2733-2019>, 2019.
- 502 Kerminen, V. M., Petäjä, T., Manninen, H. E., Paasonen, P., Nieminen, T., Sipilä, M., Junninen,
503 H., Ehn, M., Gagné, S., Laakso, L., Riipinen, I., Vehkamäki, H., Kurten, T., Ortega, I. K.,
504 Dal Maso, M., Brus, D., Hyvärinen, A., Lihavainen, H., Leppä, J., Lehtinen, K. E. J.,
505 Mirme, A., Mirme, S., Hörrak, U., Berndt, T., Stratmann, F., Birmili, W., Wiedensohler,
506 A., Metzger, A., Dommen, J., Baltensperger, U., Kiendler-Scharr, A., Mentel, T. F., Wildt,
507 J., Winkler, P. M., Wagner, P. E., Petzold, A., Minikin, A., Plass-Dülmer, C., Pöschl, U.,
508 Laaksonen, A., and Kulmala, M.: Atmospheric nucleation: Highlights of the EUCAARI
509 project and future directions, *Atmos. Chem. Phys.*, 10, 10829–10848,
510 <https://doi.org/10.5194/acp-10-10829-2010>, 2010.



- 511 Kirkby, J., Curtius, J., Almeida, J., Dunne, E., Duplissy, J., Ehrhart, S., Franchin, A., Gagné, S.,
512 Ickes, L., Kürten, A., Kupc, A., Metzger, A., Riccobono, F., Rondo, L., Schobesberger, S.,
513 Tsagkogeorgas, G., Wimmer, D., Amorim, A., Bianchi, F., Breitenlechner, M., David, A.,
514 Dommen, J., Downard, A., Ehn, M., Flagan, R. C., Haider, S., Hansel, A., Hauser, D., Jud,
515 W., Junninen, H., Kreissl, F., Kvashin, A., Laaksonen, A., Lehtipalo, K., Lima, J., Lovejoy,
516 E. R., Makhmutov, V., Mathot, S., Mikkilä, J., Minginette, P., Mogo, S., Nieminen, T.,
517 Onnela, A., Pereira, P., Petäjä, T., Schnitzhofer, R., Seinfeld, J. H., Sipilä, M., Stozhkov,
518 Y., Stratmann, F., Tomé, A., Vanhanen, J., Viisanen, Y., Virtala, A., Wagner, P. E.,
519 Walther, H., Weingartner, E., Wex, H., Winkler, P. M., Carslaw, K. S., Worsnop, D. R.,
520 Baltensperger, U., and Kulmala, M.: Role of sulphuric acid, ammonia and galactic cosmic
521 rays in atmospheric aerosol nucleation, *Nature*, 476, 429–433, [https://doi.org/](https://doi.org/10.1038/nature10343)
522 10.1038/nature10343, 2011.
- 523 Kopanakis, I., Chatoutsidou, S. E., Torseth, K., Glytsos, T., and Lazaridis, M.: Particle number
524 size distribution in the eastern Mediterranean: Formation and growth rates of ultrafine
525 airborne atmospheric particles, *Atmos. Environ.*, 77, 790–802, [https://doi.org/10.1016/](https://doi.org/10.1016/j.atmosenv.2013.05.066)
526 j.atmosenv.2013.05.066, 2013.
- 527 Kostenidou, E., Lee, B. H., Engelhart, G. J., Pierce, J. R., and Pandis, S. N.: Mass spectra
528 deconvolution of low, medium, and high volatility biogenic secondary organic aerosol,
529 *Environ. Sci. Technol.*, 43, 4884–4889, <https://doi.org/10.1021/es803676g>, 2009.
- 530 Kreidenweis, S. M., Yin, F., Wang, S.-C., Grosjean, D., Flagan, R. C., and Seinfeld, J. H.: Aerosol
531 formation during photooxidation of organosulfur species, *Atmos. Environ. Part A. Gen.*
532 *Top.*, 25, 2491–2500, [https://doi.org/10.1016/0960-1686\(91\)90165-4](https://doi.org/10.1016/0960-1686(91)90165-4), 1991.
- 533 Kulmala, M., Riipinen, I., Sipilä, M., Manninen, H. E., Petaja, T., Junninen, H., Maso, M. D.,
534 Mordas, G., Mirme, A., Vana, M., Hirsikko, A., Laakso, L., Harrison, R. M., Hanson, I.,
535 Leung, C., Lehtinen, K. E. J., and Kerminen, V.-M.: Toward Direct Measurement of
536 Atmospheric Nucleation, *Science*, 318, 89–92, <https://doi.org/10.1126/science.1144124>,
537 2007.
- 538 Kulmala, M., Petäjä, T., Nieminen, T., Sipilä, M., Manninen, H. E., Lehtipalo, K., Dal Maso, M.,
539 Aalto, P. P., Junninen, H., Paasonen, P., Riipinen, I., Lehtinen, K. E. J., Laaksonen, A., and
540 Kerminen, V. M.: Measurement of the nucleation of atmospheric aerosol particles, *Nat.*
541 *Protoc.*, 7, 1651–1667, <https://doi.org/10.1038/nprot.2012.091>, 2012.



- 542 Laaksonen, A., Pirjola, L., Kulmala, M., Wohlfrom, K. H., Arnold, F., and Raes, F.: Upper
543 tropospheric SO₂ conversion into sulfuric acid aerosols and cloud condensation nuclei, *J.*
544 *Geophys. Res. Atmos.*, 105, 1459–1469, <https://doi.org/10.1029/1999JD900933>, 2000.
- 545 Manninen, H. E., Nieminen, T., Asmi, E., Gagné, S., Häkkinen, S., Lehtipalo, K., Aalto, P., Vana,
546 M., Mirme, A., Mirme, S., Hörrak, U., Plass-Dülmer, C., Stange, G., Kiss, G., Hoffer, A.,
547 Töro, N., Moerman, M., Henzing, B., De Leeuw, G., Brinkenberg, M., Kouvarakis, G. N.,
548 Bougiatioti, A., Mihalopoulos, N., O’Dowd, C., Ceburnis, D., Arneth, A., Svenningsson,
549 B., Swietlicki, E., Tarozzi, L., Decesari, S., Facchini, M. C., Birmili, W., Sonntag, A.,
550 Wiedensohler, A., Boulon, J., Sellegri, K., Laj, P., Gysel, M., Bukowiecki, N.,
551 Weingartner, E., Wehrle, G., Laaksonen, A., Hamed, A., Joutsensaari, J., Petäjä, T.,
552 Kerminen, V. M., and Kulmala, M.: EUCAARI ion spectrometer measurements at 12
553 European sites-analysis of new particle formation events, *Atmos. Chem. Phys.*, 10, 7907–
554 7927, <https://doi.org/10.5194/acp-10-7907-2010>, 2010.
- 555 McFiggans, G., Bale, C. S. E., Ball, S. M., Beames, J. M., Bloss, W. J., Carpenter, L. J., Dorsey,
556 J., Dunk, R., Flynn, M. J., Furneaux, K. L., Gallagher, M. W., Heard, D. E., Hollingsworth,
557 A. M., Hornsby, K., Ingham, T., Jones, C. E., Jones, R. L., Kramer, L. J., Langridge, J. M.,
558 Leblanc, C., LeCrane, J. P., Lee, J. D., Leigh, R. J., Longley, I., Mahajan, A. S., Monks, P.
559 S., Oetjen, H., Orr-Ewing, A. J., Plane, J. M. C., Potin, P., Shillings, A. J. L., Thomas, F.,
560 Von Glasow, R., Wada, R., Whalley, L. K., and Whitehead, J. D.: Iodine-mediated coastal
561 particle formation: An overview of the Reactive Halogens in the Marine boundary layer
562 (RHAMBLe) Roscoff coastal study, *Atmos. Chem. Phys.*, 10, 2975–2999,
563 <https://doi.org/10.5194/acp-10-2975-2010>, 2010.
- 564 Merikanto, J., Spracklen, D. V., Mann, G. W., Pickering, S. J., and Carslaw, K. S.: Impact of
565 nucleation on global CCN, *Atmos. Chem. Phys.*, 9, 8601–8616, <https://doi.org/10.5194/acp-9-8601-2009>, 2009.
- 567 Mohr, C., Thornton, J. A., Heitto, A., Lopez-Hilfiker, F. D., Lutz, A., Riipinen, I., Hong, J.,
568 Donahue, N. M., Hallquist, M., Petäjä, T., Kulmala, M., and Yli-Juuti, T.: Molecular
569 identification of organic vapors driving atmospheric nanoparticle growth, *Nat. Commun.*,
570 10, 1–7, <https://doi.org/10.1038/s41467-019-12473-2>, 2019.
- 571 Patoulias, D., Fountoukis, C., Riipinen, I., Asmi, A., Kulmala, M., and Pandis, S. N.: Simulation
572 of the size-composition distribution of atmospheric nanoparticles over Europe, *Atmos.*



- 573 Chem. Phys., 18, 13639–13654, <https://doi.org/10.5194/acp-18-13639-2018>, 2018.
- 574 Pikridas, M., Riipinen, I., Hildebrandt, L., Kostenidou, E., Manninen, H., Mihalopoulos, N.,
575 Kalivitis, N., Burkhardt, J. F., Stohl, A., Kulmala, M., and Pandis, S. N.: New particle
576 formation at a remote site in the eastern Mediterranean, *J. Geophys. Res.*, 117, D12205,
577 <https://doi.org/10.1029/2012JD017570>, 2012.
- 578 Pope, C. A., Burnett, R. T., Thun, M. J., Calle, E. E., Krewski, D., Ito, K., and Thurston, G. D.:
579 Lung cancer, cardiopulmonary mortality, and long-term exposure to fine particulate air
580 pollution, *J. Am. Med. Assoc.*, 287, 1132–1141, <https://doi.org/10.1001/jama.287.9.1132>,
581 2002.
- 582 Saha, P. K., Zimmerman, N., Malings, C., Haurlyiuk, A., Li, Z., Snell, L., Subramanian, R.,
583 Lipsky, E., Apte, J. S., Robinson, A. L., and Presto, A. A.: Quantifying high-resolution
584 spatial variations and local source impacts of urban ultrafine particle concentrations, *Sci.*
585 *Total Environ.*, 655, 473–481, <https://doi.org/10.1016/j.scitotenv.2018.11.197>, 2019.
- 586 Siakavaras, D., Samara, C., Petrakakis, M., and Biskos, G.: Nucleation events at a coastal city
587 during the warm period: Kerbside versus urban background measurements, *Atmos.*
588 *Environ.*, 140, 60–68, <https://doi.org/10.1016/j.atmosenv.2016.05.054>, 2016.
- 589 Sipila, M., Berndt, T., Petaja, T., Brus, D., Vanhanen, J., Stratmann, F., Patokoski, J., Mauldin, R.
590 L., Hyvärinen, A. P., Lihavainen, H., and Kulmala, M.: The role of sulfuric acid in
591 atmospheric nucleation, *Science*, 327, 1243–1246, doi:10.1126/science.1180315, 2010.
- 592 Sipilä, M., Sarnela, N., Jokinen, T., Henschel, H., Junninen, H., Kontkanen, J., Richters, S.,
593 Kangasluoma, J., Franchin, A., Peräkylä, O., Rissanen, M. P., Ehn, M., Vehkamäki, H.,
594 Kurten, T., Berndt, T., Petäjä, T., Worsnop, D., Ceburnis, D., Kerminen, V. M., Kulmala,
595 M., and O’Dowd, C.: Molecular-scale evidence of aerosol particle formation via sequential
596 addition of HIO₃, *Nature*, 537, 532–534, <https://doi.org/10.1038/nature19314>, 2016.
- 597 Vratolis, S., Gini, M. I., Bezantakos, S., Stavroulas, I., Kalivitis, N., Kostenidou, E., Louvaris, E.,
598 Siakavaras, D., Biskos, G., Mihalopoulos, N., Pandis, S. N., Pilinis, C., Papayannis, A.,
599 and Eleftheriadis, K.: Particle number size distribution statistics at City-Centre Urban
600 Background, urban background, and remote stations in Greece during summer, *Atmos.*
601 *Environ.*, 213, 711–726, <https://doi.org/10.1016/j.atmosenv.2019.05.064>, 2019.
- 602 Wang, M., Kong, W., Marten, R., He, X. C., Chen, D., Pfeifer, J., Heitto, A., Kontkanen, J., Dada,
603 L., Kürten, A., Yli-Juuti, T., Manninen, H. E., Amanatidis, S., Amorim, A., Baalbaki, R.,



- 604 Baccarini, A., Bell, D. M., Bertozzi, B., Bräkling, S., Brilke, S., Murillo, L. C., Chiu, R.,
605 Chu, B., De Menezes, L. P., Duplissy, J., Finkenzeller, H., Carracedo, L. G., Granzin, M.,
606 Guida, R., Hansel, A., Hofbauer, V., Krechmer, J., Lehtipalo, K., Lamkaddam, H.,
607 Lampimäki, M., Lee, C. P., Makhmutov, V., Marie, G., Mathot, S., Mauldin, R. L.,
608 Mentler, B., Müller, T., Onnela, A., Partoll, E., Petäjä, T., Philippov, M., Pospisilova, V.,
609 Ranjithkumar, A., Rissanen, M., Rörup, B., Scholz, W., Shen, J., Simon, M., Sipilä, M.,
610 Steiner, G., Stolzenburg, D., Tham, Y. J., Tomé, A., Wagner, A. C., Wang, D. S., Wang,
611 Y., Weber, S. K., Winkler, P. M., Wlasits, P. J., Wu, Y., Xiao, M., Ye, Q., Zauner-
612 Wieczorek, M., Zhou, X., Volkamer, R., Riipinen, I., Dommen, J., Curtius, J.,
613 Baltensperger, U., Kulmala, M., Worsnop, D. R., Kirkby, J., Seinfeld, J. H., El-Haddad, I.,
614 Flagan, R. C., and Donahue, N. M.: Rapid growth of new atmospheric particles by nitric
615 acid and ammonia condensation, *Nature*, 581, 184–189, <https://doi.org/10.1038/s41586-020-2270-4>, 2020.
- 617 Wang, N., Jorga, S. D., Pierce, J. R., Donahue, N. M., and Pandis, S. N.: Particle wall-loss
618 correction methods in smog chamber experiments, *Atmos. Meas. Tech.*, 11, 6577–6588,
619 <https://doi.org/10.5194/amt-11-6577-2018>, 2018.
- 620 Wang, Z., Wu, Z., Yue, D., Shang, D., Guo, S., Sun, J., Ding, A., Wang, L., Jiang, J., Guo, H.,
621 Gao, J., Cheung, H. C., Morawska, L., Keywood, M., and Hu, M.: New particle formation
622 in China: Current knowledge and further directions, *Sci. Total Environ.*, 577, 258–266,
623 <https://doi.org/10.1016/j.scitotenv.2016.10.177>, 2017.
- 624 Weber, R. J., McMurry, P. H., Mauldin, L., Tanner, D. J., Eisele, F. L., Brechtel, F. J.,
625 Kreidenweis, S. M., Kok, G. L., Schillawski, R. D., and Baumgardner, B.: A study of new
626 particle formation and growth involving biogenic and trace gas species measured during
627 ACE 1, *J. Geophys. Res. Atmos.*, 103, 16385–16396, <https://doi.org/10.1029/97JD02465>,
628 1998.
- 629 Weber, R. J., Marti, J. J., McMurry, P. H., Eisele, F. L., Tanner, D. J., And Jefferson, A.: Measured
630 atmospheric new particle formation rates: implications for nucleation mechanisms, *Chem.*
631 *Eng. Commun.*, 151, 53–64, <https://doi.org/10.1080/00986449608936541>, 1996.
- 632 Yao, L., Garmash, O., Bianchi, F., Zheng, J., Yan, C., Kontkanen, J., Junninen, H., Mazon, S. B.,
633 Ehn, M., Paasonen, P., Sipilä, M., Wang, M., Wang, X., Xiao, S., Chen, H., Lu, Y., Zhang,
634 B., Wang, D., Fu, Q., Geng, F., Li, L., Wang, H., Qiao, L., Yang, X., Chen, J., Kerminen,



- 635 V.-M., Petäjä, T., Worsnop, D. R., Kulmala, M., and Wang, L.: Atmospheric new particle
636 formation from sulfuric acid and amines in a Chinese megacity, *Science*, 361, 278–281,
637 <https://doi.org/10.1126/science.aao4839>, 2018.
- 638 Yli-Juuti, T., Nieminen, T., Hirsikko, A., Aalto, P. P., Asmi, E., Hörrak, U., Manninen, H. E.,
639 Patokoski, J., Dal Maso, M., Petäjä, T., Rinne, J., Kulmala, M., and Riipinen, I.: Growth
640 rates of nucleation mode particles in Hyytiälä during 2003–2009: Variation with particle
641 size, season, data analysis method and ambient conditions, *Atmos. Chem. Phys.*, 11,
642 12865–12886, <https://doi.org/10.5194/acp-11-12865-2011>, 2011.
- 643 Zhao, Y., Hennigan, C. J., May, A. A., Tkacik, D. S., De Gouw, J. A., Gilman, J. B., Kuster, W.
644 C., Borbon, A., and Robinson, A. L.: Intermediate-volatility organic compounds: A large
645 source of secondary organic aerosol, *Environ. Sci. Technol.*, 48, 13743–13750,
646 <https://doi.org/10.1021/es5035188>, 2014.
- 647 Zhu, Y., Li, K., Shen, Y., Gao, Y., Liu, X., Yu, Y., Gao, H., and Yao, X.: New particle formation
648 in the marine atmosphere during seven cruise campaigns, *Atmos. Chem. Phys.*, 19, 89–
649 113, <https://doi.org/10.5194/acp-19-89-2019>, 2019.
- 650
- 651
- 652
- 653
- 654
- 655
- 656



657 **Table 1:** Initial conditions in the conducted experiments.

Exp.	Category	PM₁ ($\mu\text{g m}^{-3}$)	O₃ (ppb)	NH₃^c (ppb)	SO₂ (ppb)	NO_x (ppb)	RH (%)
Exp. A1	Class A	1.6	58	150	0.7	3.6	40
Exp. A2 ^a		4.2	47	25	1.6	12.1	50
Exp. A3 ^b		0.9	49	200	0.6	5.6	42
Exp. A4		0.6	52	120	0.5	4.4	45
Exp. A5		3.6	54	120	0.6	3.7	40
Exp. A6		3.7	52	150	1	7.2	40
Exp. B1	Class B	2.2	45	150	0.8	6.7	50
Exp. B2		1.6	49	25	1.1	8.4	56
Exp. B3		1	41	200	0.6	8.3	58
Exp. B4		2.2	56	120	0.8	4	40
Exp. C1	Class C	3	12	150	1.3	27	48
Exp. C2 ^b		2.5	56	75	0.6	7.5	38
Exp. C3 ^a		2.2	50	20	0.6	11	52

658

659 ^a Experiments illuminated by natural sunlight

660 ^b Experiment conducted at night

661 ^c Estimated concentration in the perturbation chamber.

662

663

664

665

666

667

668



669

670 **Table 2:** Nucleation time, nucleation rate and condensation rate in the experiments where NPF was
671 observed in the perturbed chamber.

Experiment	Initial GR (nm h ⁻¹)	Condensation sink × 10 ³ (s ⁻¹)	H ₂ SO ₄ × 10 ⁻⁷ (molecule cm ⁻³)
Exp. A1	4	2.6	3
Exp. A2 ^a	8	3.5	5
Exp. A3 ^b	5.5	0.8	8
Exp. A4	6.5	1.1	5
Exp. A5	3.5	3.1	2
Exp. A6	3.7	2.9	4
Exp. B1	5.5	3.1	3
Exp. B2	11.3	2.1	6
Exp. B3	7	2.4	3
Exp. B4	3.5	2	4
Exp. C1	0	2.8	5
Exp. C2 ^b	0	2.1	3
Exp. C3 ^a	0	2.5	2

672

673 ^a Experiments illuminated by natural sunlight

674 ^b Experiment conducted at night

675

676

677



678 **Table 3:** Nucleation time, nucleation rate and condensation rate in the experiments that NPF was
679 observed in the perturbed chamber.

Experiment	Nucleation time (h)	Nucleation rate ($\text{cm}^{-3} \text{h}^{-1}$)	Condensation rate (ppt h^{-1})
Exp. A1	3	9500 ± 600	3.2 ± 0.3
Exp. A2 ^a	2	10000 ± 1000	4.5 ± 0.4
Exp. A3 ^b	2	500 ± 100	3.8 ± 0.4
Exp. A4	2	600 ± 200	4.5 ± 0.3
Exp. A5	2	6500 ± 1000	2 ± 0.2
Exp. A6	3	7000 ± 500	3 ± 0.4
Exp. B1	2.5	15000 ± 1500	4.5 ± 0.5
Exp. B2	1.9	25000 ± 2000	10 ± 1
Exp. B3	2	5000 ± 700	4.5 ± 0.5
Exp. B4	2.5	14000 ± 1000	3 ± 0.2

680

681 ^a Experiments illuminated by natural sunlight

682 ^b Experiment conducted at night

683

684

685

686

687

688



689

690

691

692

693

694

695

696

697

698

699

700

701

702

703

704

705

706

707

708

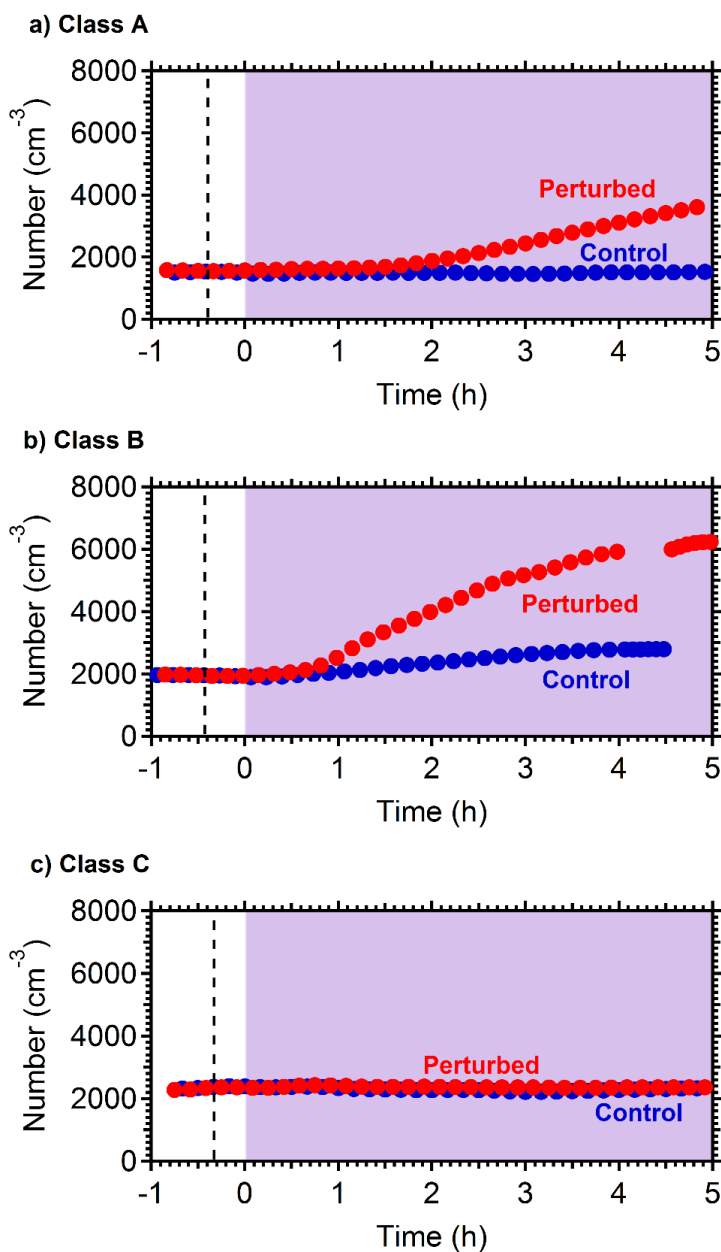
709

710

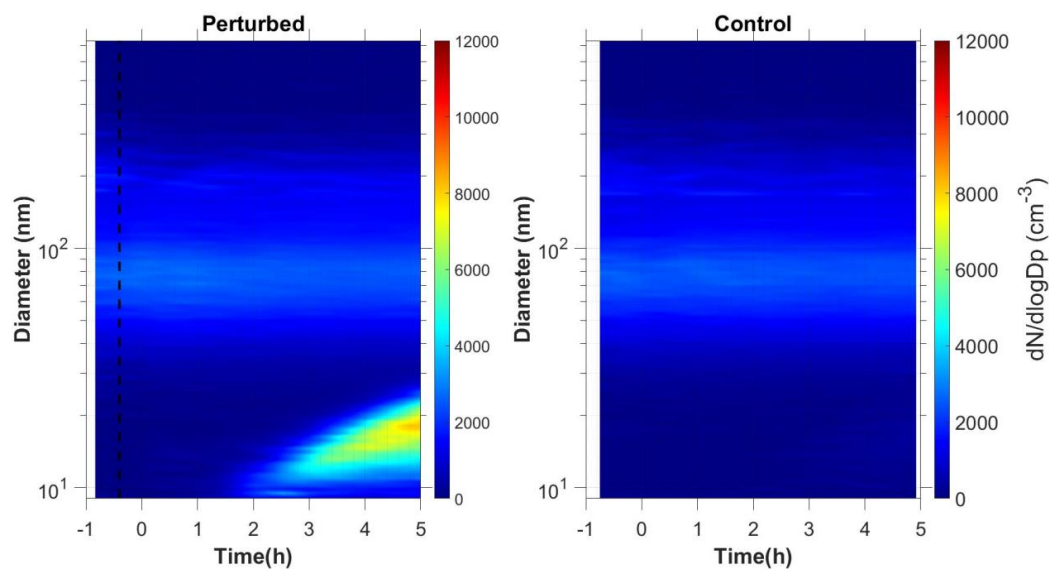
711

712

713



714 **Figure 1:** Wall loss corrected number concentration N_9 in the three different types of experiments,
715 a) NPF and growth only in the perturbed chamber (Exp. A1), b) NPF and growth in both chambers
716 (Exp. B1) and c) no NPF observed (Exp. C1). The dashed line marks the time that ammonia was
717 injected in the perturbed chamber. At $t=0$ both chambers were illuminated with UV light.



718

719 **Figure 2:** Wall loss corrected measured number distributions in the two chambers for Exp. A1.

720

721

722

723

724

725

726

727

728

729

730

731

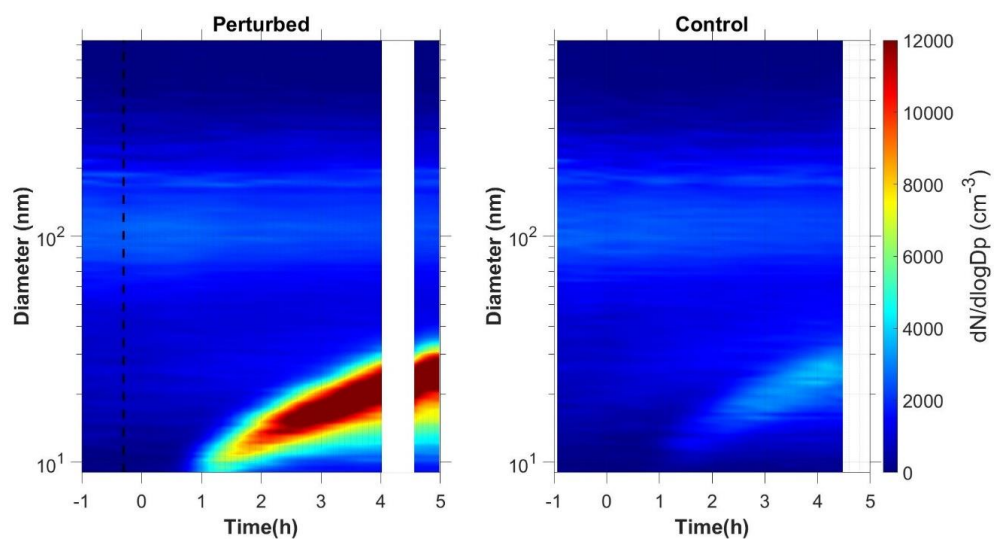
732

733

734



735



736

737 **Figure 3:** Wall loss corrected measured number distributions in the two chambers for Exp. B1.

738

739

740

741

742

743

744

745

746

747

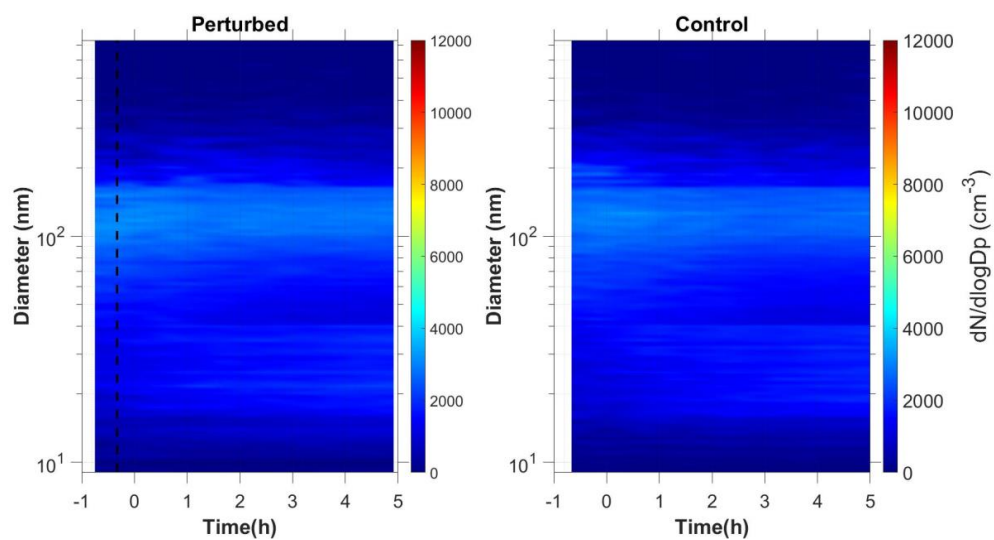
748

749

750



751



752 **Figure 4:** Wall loss corrected measured number distributions in the two chambers for Exp. C1.

753

754

755

756

757

758

759

760

761

762

763

764

765

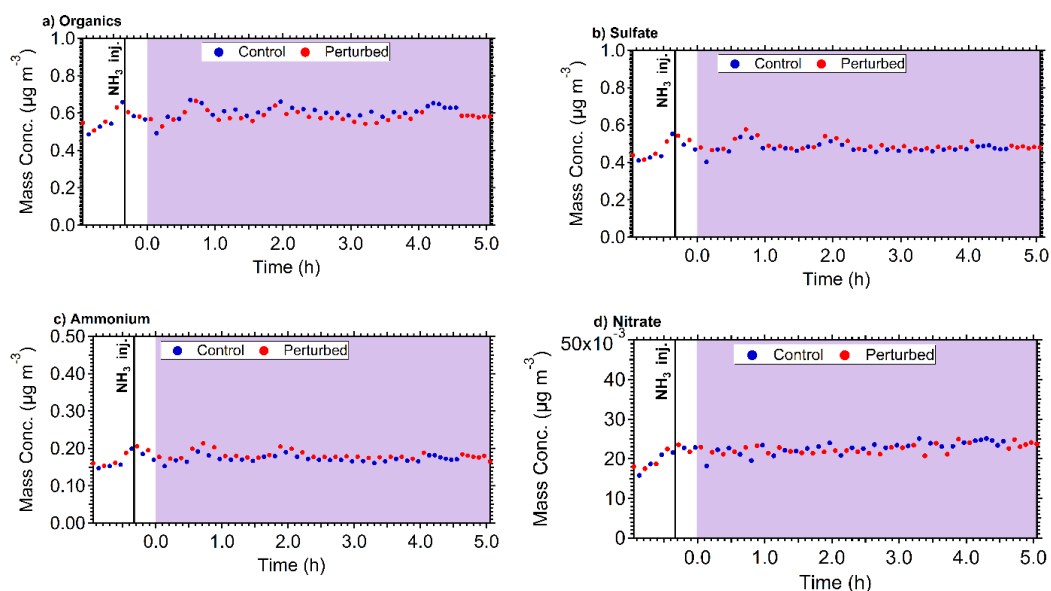
766

767

768



769



770

771 **Figure 5:** The wall loss corrected mass concentration of a) organics, b) sulfate, c) ammonium and
772 d) nitrate in the control (blue dots) and perturbed (red dots) chamber during Exp. B1. The purple
773 shades region represents the time that the chambers were under UV illumination.

774

775

776

777

778

779

780

781

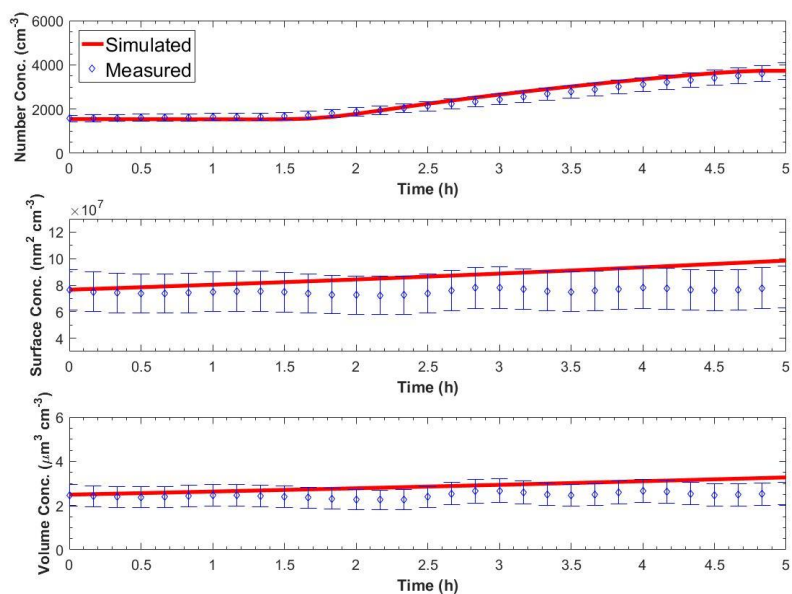
782

783

784

785

786



787 **Figure 6:** Measured and simulated number, surface and volume concentration in the perturbed
788 chamber after turning UV lights on for Exp. A1. The error bars in the measured values are
789 calculated from the uncertainty in the particle wall loss correction and represent two standard
790 deviations.

791